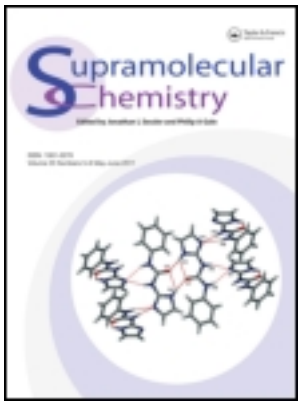

Supramolecular Chemistry
Publication details, including instructions for authors and subscription information:
http://www.tandfonline.com/loi/gsch20

Structure and selectivity trends in crystalline urea-functionalised anion-binding capsules

Arbin Rajbanshi [a] & Radu Custelcean [a]
[a] Chemical Sciences Division, Oak Ridge National Laboratory, Oak Ridge, TN, 37831, USA

Available online: 03 Nov 2011

To cite this article: Arbin Rajbanshi & Radu Custelcean (2012): Structure and selectivity trends in crystalline urea-functionalised anion-binding capsules, Supramolecular Chemistry, 24:1, 65-71

To link to this article: http://dx.doi.org/10.1080/10610278.2011.622387

Supramolecular Chemistry
Vol. 24, No. 1, January 2012, 65–71

Structure and selectivity trends in crystalline urea-functionalised anion-binding capsules

Arbin Rajbanshi and Radu Custelcean*

Chemical Sciences Division, Oak Ridge National Laboratory, Oak Ridge, TN 37831, USA

(*Received 29 June 2011; final version received 5 September 2011*)

A tripodal trisurea receptor (**L1**) persistently self-assembles with various divalent oxoanion salts M_nX (M = Na, K, Mg, Ca, Cd; X = SO_4^{2-}, SO_3^{2-}, SeO_4^{2-}, CrO_4^{2-}) into isomorphous series of crystalline frameworks in three different compositions: $MX(\mathbf{L1})_2(H_2O)_6$ (M = Mg, Ca, Cd) (**1**), $Na_2X(\mathbf{L1})_2(H_2O)_4$ (**2**) and $K_2X(\mathbf{L1})_2(H_2O)_2$ (**3**). Single-crystal X-ray structural analysis revealed that all three series of structures adopt a NaCl-type topology, consisting of alternating anionic $X(\mathbf{L1})_2^{2-}$ capsules and $M(H_2O)_6^{2+}$, $Na_2(H_2O)_4^{2+}$ or $K_2(H_2O)_2^{2+}$ hydrated cations. The capsules provide a complementary environment to tetrahedral oxoanions via 12 hydrogen bonds from six urea groups lining the cavities of the capsules. The persistent formation of the capsules facilitated the investigation of structural trends and structure–selectivity relationships across series **1**–**3**. First, it was found that the size of the capsules is relatively unresponsive to the change in the encapsulated anion, resulting in good shape and size recognition in the separation of anions by competitive crystallisations. Second, it was found that the size of the capsules varies linearly with the size of the external cation, which provides a way for tuning the anion encapsulation selectivity. However, no straightforward dependence was found between the size of the capsules and the relative selectivity for different-sized tetrahedral oxoanions in competitive crystallisations.

Keywords: anion recognition; crystal engineering; hydrogen bonding; self-assembled capsules

1. Introduction

As recognised from the dawn of supramolecular chemistry of anions (*1–3*), effective recognition and separation of strongly hydrophilic anions from competitive aqueous environments require encapsulation inside relatively rigid cage-like receptors with complementary binding cavities (*4*, *5*). Like in natural protein receptors, anion encapsulation ensures efficient shielding from the water solvent, resulting in enhanced anion-binding strength and selectivity. A generally perceived limitation with cage receptors (*6*) is that their assembly is typically laborious and inefficient, requiring multistep syntheses and tedious purifications. A more practical approach is to employ self-assembly to build anion-binding cages from simple building blocks (*7*). The cage self-assembly can be induced by the anion (*8*) or/and can be assisted by metal coordination (*9*). The design of building blocks functionalised with strong and specific anion-binding groups that upon self-assembly converge inside well-defined and complementary cavities can result in tight and selective anion encapsulation (*10*). Alternatively to solution self-assembly, anion-binding cages can be self-assembled in the solid state through crystallisation (*11–13*). The latter approach offers the additional advantage of enhanced organisational rigidity characteristic to the crystalline state, which may lead to superior anion selectivities as the binding sites cannot easily adjust their structures to accommodate unwanted competing anions.

Following our first report of anion recognition and separation by competitive crystallisation of supramolecular frameworks functionalised with anion-binding groups (*14*), a number of other studies demonstrating this concept have been published (*15–25*). The rationalisation of the observed anion selectivities in many such studies is complicated by the fact that completely different crystal structures are often formed from the various anions under study. In such cases, in addition to differences in the anion coordination, a multitude of other factors can contribute to anion selectivity, such as crystal packing, the nature and dimensionality of the supramolecular motifs manifested in the crystals, and the nature of chemical groups exposed on the crystal faces. The interpretation of the observed selectivities is greatly simplified when all anions studied form isomorphous or isostructural crystals (same space group and crystal packing, and similar lattice parameters), as in such cases the anion selectivities are primarily determined by the anion coordination at the binding sites.

Previous studies (*26–29*) showed that the urea-functionalised tripodal ligand tris[2-(3-pyridylurea)ethyl]-amine **L1** (Scheme 1) self-assembles in the presence of divalent metal sulphate salts, MSO_4 (M = Mg, Zn, Cd, Co, Mn) in water/methanol mixtures to give 3D

*Corresponding author. Email: custelceanr@ornl.gov

ISSN 1061-0278 print/ISSN 1029-0478 online

http://dx.doi.org/10.1080/10610278.2011.622387
http://www.tandfonline.com

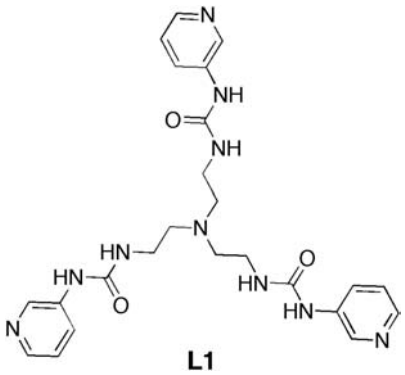

Scheme 1. Tripodal trisurea ligand **L1**.

crystalline frameworks with the composition $MSO_4(\mathbf{L1})_2(H_2O)_6$ (**1**).

All crystals in this series were found to have isomorphous structures with anionic $SO_4(\mathbf{L1})_2^{2-}$ capsules and cationic $M(H_2O)_6^{2+}$ units linked into hydrogen-bonded frameworks with NaCl-type topology (Figure 1). Very recently, we found that the monovalent cations Na^+ and K^+ can form similar NaCl-type frameworks, where the $M(H_2O)_6^{2+}$ units are replaced by $Na_2(H_2O)_4^{2+}$ or $K_2(H_2O)_2^{2+}$ cationic clusters to form crystals with the composition $Na_2SO_4(\mathbf{L1})_2(H_2O)_4$ (**2**) and $K_2SO_4(\mathbf{L1})_2(H_2O)_2$ (**3**), respectively (Figure 1) (*30*). However, a different structure was observed in the $Li_2SO_4(\mathbf{L1})_2(H_2O)_2$ crystal, which adopted a pyrite-type topology (*31*).

The sulphate anion in all these crystals is encapsulated by two embracing **L1** ligands providing 12 hydrogen bonds from six urea anion-binding groups (*32*). This binding environment is highly complementary to the tetrahedral SO_4^{2-}, as well as the similarly shaped but slightly larger SeO_4^{2-}, while anions of different shapes, such as the trigonal pyramidal SO_3^{2-} or trigonal planar CO_3^{2-}, do not fit well inside the capsules, engaging in repulsive NH···S and NH···C interactions. As a result, good selectivity for the tetrahedral SO_4^{2-} and SeO_4^{2-} against SO_3^{2-} and CO_3^{2-} was observed in the competitive crystallisation experiments with the Mg-based system, though the SO_4^{2-} versus SeO_4^{2-} size discrimination was modest (*26*, *27*). However, it is difficult to draw definitive conclusions and enunciate general principles based on this

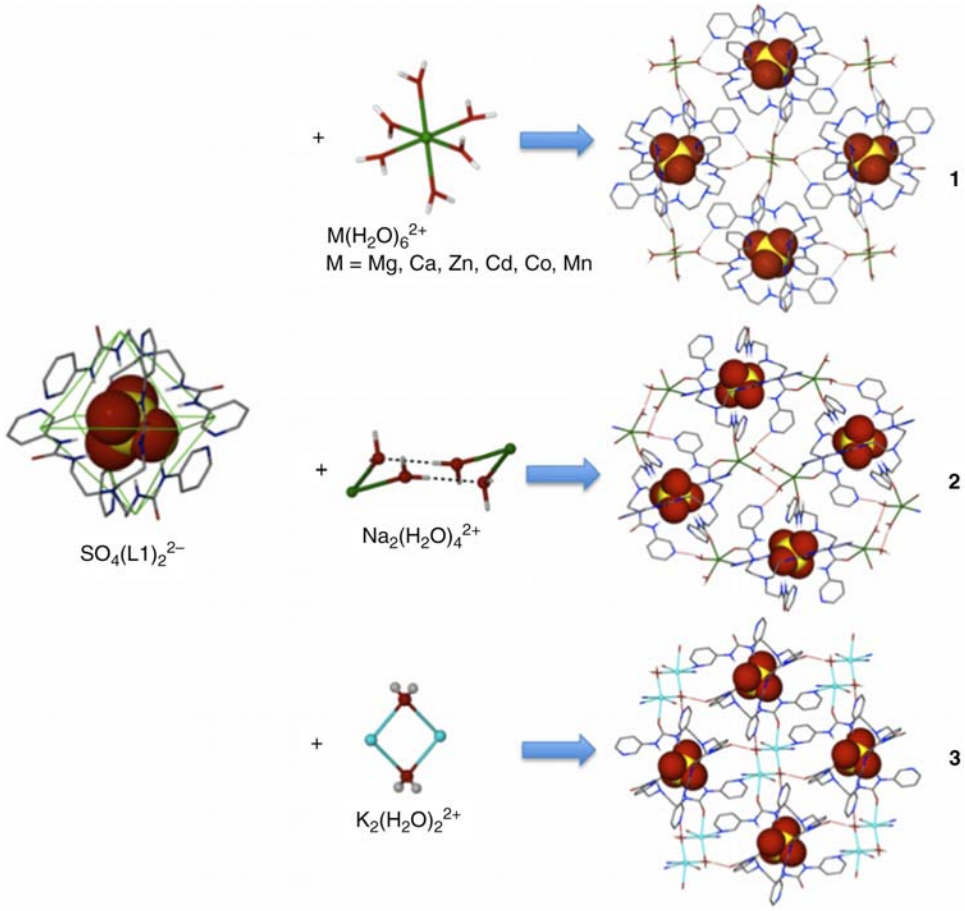

Figure 1. Self-assembly of the anionic capsule $SO_4(\mathbf{L1})_2^{2-}$ with $M(H_2O)_6^{2+}$, $Na_2(H_2O)_4^{2+}$ or $K_2(H_2O)_2^{2+}$ cationic clusters into crystalline supramolecular frameworks with NaCl-type structures.

system alone. In this paper, we report a more extensive analysis looking at structural trends and structure–selectivity relationships across the whole series of crystalline capsules. First, we looked at structural trends across series **1**–**3**, paying particular attention to the influence of the encapsulated anions as well as external cations on the structure of the capsules. Next, we investigated the shape selectivity in the $Na_2X(\mathbf{L1})_2(H_2O)_4$ system ($X = SO_4^{2-}$, SO_3^{2-}, CO_3^{2-}) in comparison with the previously reported $MgX(\mathbf{L1})_2(H_2O)_6$ system (*26*, *27*). Finally, the size selectivity between tetrahedral oxoanions (SO_4^{2-}/SeO_4^{2-} and SO_4^{2-}/CrO_4^{2-}) was analysed as a function of the size of the capsules across series **1**–**3**.

2. Results and discussion

2.1 Structural trends in the crystalline capsules

The tripodal trisurea ligand **L1** crystallises with divalent metal sulphate salts MSO_4 (M = Mg, Zn, Cd, Co, Mn) from water/methanol mixtures into isomorphous crystalline frameworks with the composition $MSO_4(\mathbf{L1})_2(H_2O)_6$ (**1**). The Mg-based system (**1a**) had been studied in detail and found to form similar structures with SO_3^{2-}, CO_3^{2-} and SeO_4^{2-} (*26*, *27*). We have now expanded this series to include the corresponding isomorphous structures of $MgCrO_4$ (**1a**-CrO_4), $CaSO_4$ (**1b**-SO_4), $CaSeO_4$ (**1b**-SeO_4), $CaCrO_4$ (**1b**-CrO_4), $CdSeO_4$ (**1c**-SeO_4) and $CdCrO_4$ (**1c**-CrO_4). The Na- and K-based series, with the prototype structures $Na_2SO_4(\mathbf{L1})_2(H_2O)_4$ (**2**-SO_4) and $K_2SO_4(\mathbf{L1})_2(H_2O)_2$ (**3**-SO_4) (*30*), were also expanded with the corresponding isomorphous crystal structures of Na_2SO_3 (**2**-SO_3), Na_2SeO_4 (**2**-SeO_4), Na_2CrO_4 (**2**-CrO_4) and K_2SeO_4 (**3**-SeO_4), K_2CrO_4 (**3**-CrO_4), respectively.

This wealth of crystal structure data provided an opportunity for analysing structural trends in this class of crystalline anion-binding capsules. Two separate analyses were performed to identify the individual influences of the anion and the cation on the structure of the capsules. First, we looked at the Na-based system (**2**) by keeping the cation constant and varying the anions (SO_4^{2-}, SO_3^{2-}, SeO_4^{2-} and CrO_4^{2-}). Second, we looked across the series **1**–**3** by keeping the anion constant (SO_4^{2-}) and varying the cations (Na, K, Mg, Ca and Cd).

The four crystal structures in the Na series (**2**-SO_4^{2-}, **2**-SO_3^{2-}, **2**-SeO_4^{2-} and **2**-CrO_4^{2-}) are isomorphous, displaying the $P2_1/n$ space group and very similar unit cell dimensions. They consist of alternating anionic $X(\mathbf{L1})_2^{2-}$ capsules and cationic $Na_2(H_2O)_4^{2+}$ clusters linked together by water hydrogen bonding and Na coordination in a 3D NaCl-type framework (Figure 1). Figure 2 depicts the anion-binding capsules found in these crystals. They consist of two embracing **L1** ligands coordinating the encapsulated anions by 12 NH hydrogen bonds from six urea groups, as previously found in analogous structures. The SO_3^{2-} anion is also engaged in repulsive interactions between two urea NH groups and the S atom (shown as dotted lines in Figure 2(b)) with observed NH···S contact distances of 2.90 and 2.97 Å. The encapsulated anions display twofold disorder, as a result of the centrosymmetric structures of the capsules enforced by the crystal symmetry.

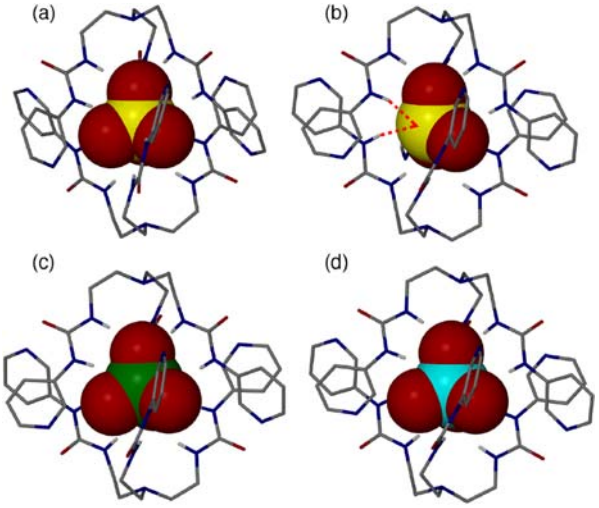

Figure 2. Anion-binding sites in the crystal of **2**-SO_4^{2-} (a), **2**-SO_3^{2-} (b), **2**-SeO_4^{2-} (c) and **2**-CrO_4^{2-} (d). The dotted lines in **2**-SO_3^{2-} represent repulsive NH···S interactions.

Figure 3 presents an overlay of the four capsules in this series, showing that they are almost identical in size and shape. The heights of the capsules measured between the bridgehead N atoms of the two **L1** ligands vary only slightly, by 0.05 Å, between the four structures. Evidently, the structures of the capsules in this series are relatively insensitive to the nature of the anion, as also noted in the Mg series, where the capsule height changed by only 0.06 Å

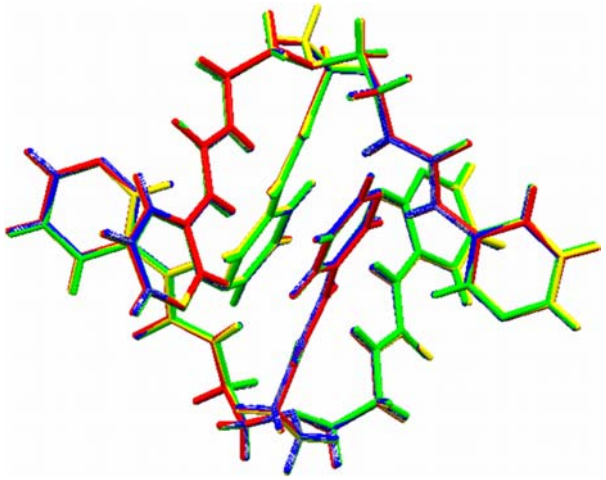

Figure 3. Overlay of the structures of the capsules in **2**-SO_4^{2-}, **2**-SO_3^{2-}, **2**-SeO_4^{2-} and **2**-CrO_4^{2-}.

between different anions. Similarly, the corresponding size of the capsules in the Ca (**1b**) and Cd (**1c**) series only varies by 0.05 and 0.04 Å, respectively, with the change in the anions. Thus, despite the inherently flexible nature of **L1**, the capsules show remarkable organisational rigidity in the crystalline state, which is likely a contributing factor to the observed anion selectivity in competitive crystallisations, as discussed in the following section.

In contrast to the negligible effect of the encapsulated anion, the external cation exerts a much stronger influence over the structure of the capsules. In particular, the height of the capsules varies from 9.20 to 9.83 Å between the smallest $K_2(H_2O)_2^{2+}$ and the largest $Ca(H_2O)_6^{2+}$ cationic clusters (Figure 4).

There is a good linear correlation ($R^2 = 0.90$) between the capsule height and the volume of the external cationic cluster (Figure 5(a)). The correlation is even stronger ($R^2 = 0.98$) if the surface area of the cations is plotted instead of their volumes (Figure 5(b)). These correlations could be explained in terms of close-packing effects. As depicted in Figure 6, the anionic capsules pack closely around the cation in the crystals as they try to minimise the void space and optimise the van der Waals interactions. Interestingly, the same close packing of the capsules was observed regardless of the nature and size of the cations. It thus follows that as a larger cation is replaced by a smaller one in the series, the capsules shrink so they can pack closer and fill the void corresponding to the difference between the cations' volumes. As the path of least resistance is apparently along the N—N axis of the capsules, this distance varies most substantially in response to the change in cation. To summarise the structural response in this class of crystalline capsules, for a given cation, the structure of the capsules is relatively insensitive to the nature of the encapsulated anion, but it varies significantly with the change in the external cation. In the following section, the implications of these structural trends to anion selectivity in competitive crystallisations are analysed.

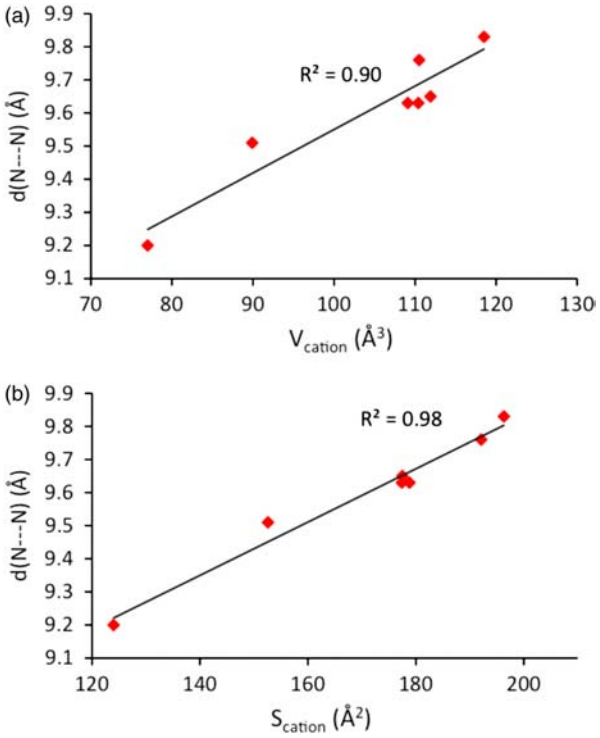

Figure 5. Plots of the height of the capsules versus volume (a) or surface area (b) of the external cations. The values for the volume of cations and surface area were calculated using the Spartan'08 software.

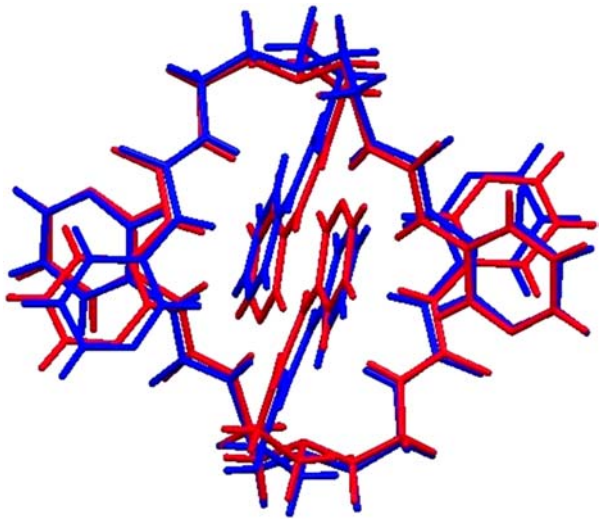

Figure 4. Overlay of the structures of the capsules in **1b**-SO_4 and **3**-SO_4.

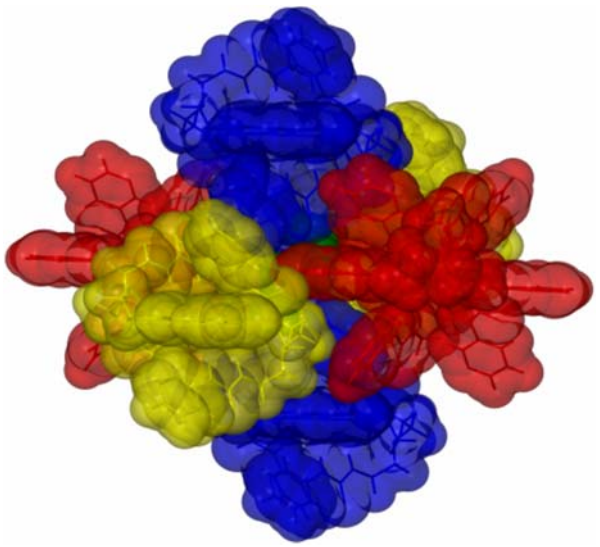

Figure 6. Close packing of the capsules in the crystals of **1**–**3**.

2.2. *Selectivity trends in competitive crystallisations of the capsules*

As described in the previous section, the detailed structural investigation of the Na-based system **2** indicated that the capsules are a good fit for the tetrahedral SO_4^{2-}, SeO_4^{2-} and CrO_4^{2-} anions as a result of 12 complementary hydrogen bonds from the six urea groups lining the cavities. The pyramidal-shaped SO_3^{2-}, on the other hand, did not fit so well inside the capsules, engaging in repulsive NH···S interactions. Though we do not have the crystal structure of the Na capsule with CO_3^{2-}, we assume this anion also engages in repulsive NH···C interactions, as previously found in the Mg-based system **1a** (*26*, *27*). The capsules in **2** also showed a high degree of organisational rigidity, displaying minimal structural variation with the change in the encapsulated anion. For these reasons, we expected that the capsules would show good shape recognition for tetrahedral oxoanions in the crystalline state. To test this hypothesis, we performed pairwise competitive crystallisation experiments with **L1** (two equivalents), one equivalent of Na_2SO_4 and one equivalent of Na_2SO_3 or Na_2CO_3, in H_2O/MeOH solutions. The resulting crystals were analysed by powder X-ray diffraction (PXRD) and Fourier Transform Infrared (FTIR) spectroscopy, which revealed the formation of crystalline **2** containing SO_4^{2-} as the major anion. The elemental analysis of the same crystalline solids showed the anion selectivity to follow the order $SO_4^{2-} > SO_3^{2-} > CO_3^{2-}$ with observed molar ratios of sulphate over the competing sulphite and carbonate anions of 5.9 and 11.5, respectively. These results are qualitatively similar with the previous findings from the selective crystallisation of **1a**, although the observed sulphate over sulphite and carbonate selectivity in **2** was somewhat lower. This could be attributed to the difference in the repulsive NH···S and NH···C contact distances in **1** and **2**. Thus, although the observed NH···S contact distance in **1a** was found to be 2.75 Å, which is 0.25 Å shorter than the sum of the van der Waals radii of H and S, the corresponding NH···S contact distance in **2** is 2.90 Å. Such a longer contact distance, only 0.1 Å below the sum of the van der Waals radii of the contact atoms, is presumably associated with a less unfavourable binding of SO_3^{2-}, thereby resulting in lower SO_4^{2-}/SO_3^{2-} selectivity in **2**.

To assess the size recognition of the crystalline capsule **2**, similar pairwise competitive crystallisation experiments were performed with **L1** (two equivalents) and Na_2SO_4/Na_2SeO_4 mixtures (one equivalent each) in H_2O/MeOH. The SO_4^{2-} versus SeO_4^{2-} competition is ideal for probing the size selectivity, as these two anions have the same tetrahedral shape, very similar basicities (p*K*a = 1.99 and 1.70 for HSO_4^- and $HSeO_4^-$, respectively), but slightly different sizes ($d_{S-O} = 1.49$ Å, $d_{Se-O} = 1.65$ Å). The SO_4^{2-}/SeO_4^{2-} molar ratio found in the crystalline solid resulting from the competitive crystallisation of **2** was 31.3, indicating strong size recognition for SO_4^{2-}. The observed sulphate preference in **2** is much more pronounced than in the Mg system **1a**, which displayed a corresponding SO_4^{2-}/SeO_4^{2-} ratio of only 3. The increased SO_4^{2-}/SeO_4^{2-} selectivity in **2** may be rationalised based on the smaller size of the Na capsule (d(N···N) = 9.51 Å) compared to the Mg capsule (d(N···N) = 9.65 Å), which favoured the smaller sulphate anion.

In comparison with the good SO_4^{2-}/SeO_4^{2-} selectivity observed in the crystallisation of **2**, the competitive crystallisation experiment involving a Na_2SO_4/Na_2CrO_4 mixture under similar conditions yielded crystals with a SO_4^{2-}/CrO_4^{2-} ratio of only 2.0. First, this may seem surprising, given that chromate has a size almost identical to selenate ($d_{Cr-O} = 1.64$ Å). However, one has to take into consideration the much higher basicity of CrO_4^{2-} (p*K*a($HCrO_4^-$) = 6.51). As a result, binding of chromate is inherently favoured due to its stronger hydrogen bond acceptor ability compared to sulphate, a factor that apparently offsets much of the size discrimination effect.

Next, we analysed SO_4^{2-}/SeO_4^{2-} and SO_4^{2-}/CrO_4^{2-} selectivities observed in competitive crystallisations across **1–3** series as a function of the size of the capsules. The results are summarised in Table 1 and plotted in Figure 7. The size of the capsules, measured as the N···N distance, increases in the order K < Na < Mg < Cd < Ca. However, the corresponding SO_4^{2-}/SeO_4^{2-} and SO_4^{2-}/CrO_4^{2-} selectivities do not monotonously follow the same order. It

Table 1. Anion selectivities (as SO_4^{2-}/SeO_4^{2-} and SO_4^{2-}/CrO_4^{2-} molar ratios in the crystals) found in the sulphate/selenate and sulphate/chromate competitive crystallisations across **1–3** series.

Cation	d(N···N)/Å	SO_4^{2-}/SeO_4^{2-}	SO_4^{2-}/CrO_4^{2-}
$K_2(H_2O)_2^{2+}$(**3**)	9.21	13.3	1.1
$Na_2(H_2O)_4^{2+}$(**2**)	9.51	31.3	2.0
$Mg(H_2O)_6^{2+}$(**1a**)	9.65	3.0	0.7
$Cd(H_2O)_6^{2+}$(**1c**)	9.76	6.0	0.7
$Ca(H_2O)_6^{2+}$(**1b**)	9.86	8.4	0.7

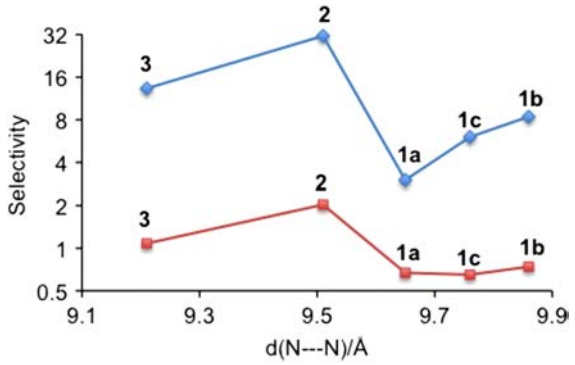

Figure 7. SO_4^{2-}/SeO_4^{2-} (diamonds) and SO_4^{2-}/CrO_4^{2-} (squares) selectivities as a function of the height of the capsules in the competitive crystallisations of **1–3**.

becomes thus obvious that size alone cannot explain the selectivity trend observed. Other factors, such as ion solvation, ion pairing, enthalpy–entropy compensations or kinetics, may need to be taken into account to rationalise these results. For example, for the Mg system, detailed thermodynamic studies indicated that entropy plays a critical role in the crystallisation of the capsules, showing an opposite effect to enthalpy, and essentially controlling the observed anion selectivity order (*27*). Until similar studies are carried out for the other crystalline capsules in the series, no definitive conclusions about the underlying cause for the observed anion selectivity trends can be reached.

3. Experimental

All reagents and solvents were purchased from commercial suppliers and used without further purification. Melting points were measured on a Uni-Melt Thomas Hoover capillary melting point apparatus and are uncorrected. PXRD patterns were obtained at room temperature on a Bruker D5005 diffractometer using monochromatic Cu Kα radiation ($\lambda = 1.5418$ Å). FTIR spectra were recorded in KBr pellets using a Digilab FTS 7000 spectrometer. Elemental analyses were performed by Galbraith Laboratories, Inc. **L1**·2H_2O was synthesised according to a previously published procedure (*30*, *31*). Single-crystal X-ray data were collected on a Bruker SMART APEX CCD diffractometer with fine-focus Mo Kα radiation ($\lambda = 0.71073$ Å), operated at 50 kV and 30 mÅ. The structures were solved by direct methods and refined on F^2 using the SHELXTL software package (SHELXTL 6.12, 1997; Bruker AXS, Inc., Madison, WI, USA). Absorption corrections were applied using SADABS, part of the SHELXTL package. All non-hydrogen atoms were refined anisotropically. Hydrogen atoms were placed in idealised positions and refined with a riding model, except for the water protons, which were located from the difference Fourier maps and refined isotropically. Crystallographic details for **1a**-CrO_4 (CCDC 831932), **1b**-CrO_4 (CCDC 831933), **1b**-SeO_4 (CCDC 831934), **1b**-SO_4 (CCDC 831935), **1c**-CrO_4 (CCDC 831936), **1c**-SeO_4 (CCDC 831937), **2**-CrO_4 (CCDC 831938), **2**-SeO_4 (CCDC 831939), **2**-SO_3 (CCDC 831940), **3**-CrO_4 (CCDC 831941) and **3**-SeO_4 (CCDC 831942) are included in the Supplementary Information available online.

3.1 Crystallisation experiments

Single crystals of **1** were obtained by crystallisation of **L1**·2H_2O (two equivalents), $M(NO_3)_2$ ($M = Mg^{2+}$, Ca^{2+}, Cd^{2+}; one equivalent) and Na_2X ($X = SO_4^{2-}$, CrO_4^{2-}, SeO_4^{2-}; one equivalent) from H_2O/MeOH solutions (1:1, v/v) at room temperature. Single crystals of **2** and **3** were obtained by crystallisation of **L1**·2H_2O (two equivalents) and M_2X ($M = Na^+$, K^+; $X = SO_4^{2-}$, SO_3^{2-}, CrO_4^{2-}, SeO_4^{2-}; one equivalent) from H_2O/MeOH solutions (1:1, v/v) at room temperature. The resulting crystals were filtered after a few days, washed with water and dried. Their structures were determined by single-crystal X-ray diffraction (Supplementary Information available online). The phase purity of the crystalline solids **1**–**3** was verified by PXRD, which yielded powder patterns that coincided with the simulated patterns from the single-crystal X-ray data. The crystalline solids **2** and **3** were additionally characterised by FTIR spectroscopy and melting point measurements:

*$Na_2SO_4(L1)_2(H_2O)_4$ (**2**-SO_4).* Colourless prisms. MP: 170–172°C. FTIR (KBr): $\nu = 1095\ cm^{-1}$ (SO_4^{2-}).

*$Na_2SO_3(L1)_2(H_2O)_4$ (**2**-SO_3).* Colourless plates. MP: 165–166°C. FTIR (KBr): $\nu = 953\ cm^{-1}$ (SO_3^{2-}).

*$Na_2CrO_4(L1)_2(H_2O)_4$ (**2**-CrO_4).* Yellow prisms. MP: 195°C (dec). FTIR (KBr): $\nu = 876\ cm^{-1}$ (CrO_4^{2-}).

*$Na_2SeO_4(L1)_2(H_2O)_4$ (**2**-SeO_4).* Colourless prisms. MP: 170–171°C. FTIR (KBr): $\nu = 870\ cm^{-1}$ (SeO_4^{2-}).

*$K_2SO_4(L1)_2(H_2O)_2$ (**3**-SO_4).* Colourless plates. MP: 186–188°C. FTIR (KBr): $\nu = 1098\ cm^{-1}$ (SO_4^{2-}).

*$K_2CrO_4(L1)_2(H_2O)_2$ (**3**-CrO_4).* Yellow prisms. MP: 205–206°C. FTIR (KBr): $\nu = 878\ cm^{-1}$ (CrO_4^{2-}).

*$K_2SeO_4(L1)_2(H_2O)_2$ (**3**-SeO_4).* Colourless plates. MP: 185°C (dec). FTIR (KBr): $\nu = 868\ cm^{-1}$ (SeO_4^{2-}).

3.1.1 General procedure for competitive crystallisations of *1*

To a solution containing one equivalent of $M(NO_3)_2$ (M = Mg, Ca, Cd), one equivalent of Na_2SO_4 and one equivalent of Na_2CrO_4 or Na_2SeO_4 in water, two equivalents of **L1**·2H_2O in MeOH were added. The resulting H_2O/MeOH (10:1, v/v) solution was stirred with a vortexer at room temperature for 5 days, and the resulting precipitate was filtered, washed with water and dried. The crystalline products were characterised by FTIR spectroscopy, PXRD and elemental analysis:

$[Mg(SO_4)_{0.4}(CrO_4)_{0.6}(L1)_2(H_2O)_6]$. FTIR (KBr): $\nu = 1094\ cm^{-1}$ (SO_4^{2-}), 874, 899 cm^{-1} (CrO_4^{2-}); analysis calculated (%): C, 45.99; H, 5.79; N, 22.35; S, 1.02; Cr, 2.49. Found: C, 45.61; H, 5.71; N, 22.60; S, 0.97; Cr, 2.48. SO_4^{2-}/CrO_4^{2-} (mol/mol) = 0.67.

$[Ca(SO_4)_{0.894}(SeO_4)_{0.106}(L1)_2(H_2O)_6]$. FTIR (KBr): $\nu = 1095\ cm^{-1}$ (SO_4^{2-}), 875 cm^{-1} (SeO_4^{2-}); analysis calculated (%): C, 45.67; H, 5.75; N, 22.19; Ca, 3.17; S, 2.27; Se, 0.66. Found: C, 45.17; H, 5.54; N, 21.69; Ca, 2.98; S, 2.13; Se, 0.62. SO_4^{2-}/SeO_4^{2-} (mol/mol) = 8.4.

$[Ca(SO_4)_{0.425}(CrO_4)_{0.575}(L1)_2(H_2O)_6]$. FTIR (KBr): $\nu = 1095\ cm^{-1}$ (SO_4^{2-}), 873, 894 cm^{-1} (CrO_4^{2-}); analysis calculated (%): S, 1.01; Cr, 2.21. SO_4^{2-}/CrO_4^{2-} (mol/mol) = 0.74.

$[Cd(SO_4)_{0.858}(SeO_4)_{0.142}(L1)_2(H_2O)_6]$. FTIR (KBr): $\nu = 1094\ cm^{-1}$ (SO_4^{2-}), 869 cm^{-1} (SeO_4^{2-}); analysis calculated (%): C, 43.14; H, 5.43; N, 20.96; Cd, 8.41; S, 2.06;

Se, 0.84. Found: C, 42.20; H, 5.12; N, 20.03; Cd, 7.87; S, 1.92; Se, 0.78. SO_4^{2-}/SeO_4^{2-} (mol/mol) = 6.04.

[Cd(SO$_4$)$_{0.395}$(CrO$_4$)$_{0.605}$(L1)$_2$(H$_2$O)$_6$]. FTIR (KBr): $\nu = 1094\,cm^{-1}$ (SO_4^{2-}), $865\,cm^{-1}$ (CrO_4^{2-}); analysis calculated (%): S, 1.23; Cr, 3.05. SO_4^{2-}/CrO_4^{2-} (mol/mol) = 0.65.

3.1.2. General procedure for competitive crystallisations of **2** and **3**

To a solution containing one equivalent of M_2SO_4 (M = Na, K) and one equivalent of M_2X (X = SO_3, CO_3, CrO_4, SeO_4) in water, two equivalents of **L1**·2H$_2$O in MeOH were added. The resulting H$_2$O/MeOH (2:1, v/v) solution was then allowed to crystallise by slow evaporation at room temperature. The resulting crystals were filtered, washed with water and dried. The crystalline products were characterised by FTIR spectroscopy, PXRD and elemental analysis:

[Na$_2$(SO$_4$)$_{0.856}$(SO$_3$)$_{0.144}$(L1)$_2$(H$_2$O)$_4$]. FTIR (KBr): $\nu = 1095\,cm^{-1}$ (SO_4^{2-}), $953\,cm^{-1}$ (SO_3^{2-}); analysis calculated (%): C, 47.07; H, 5.60; N, 22.87; Na, 3.75; S, 2.62; sulphite, 0.942. Found: C, 47.97; H, 5.34; N, 23.20; Na, 3.99; S, 2.44; sulphite, 0.94. SO_4^{2-}/SO_3^{2-} (mol/mol) = 5.9.

[Na$_2$(SO$_4$)$_{0.92}$(CO$_3$)$_{0.08}$(L1)$_2$(H$_2$O)$_4$]. FTIR (KBr): $\nu = 1095\,cm^{-1}$ (SO_4^{2-}); analysis calculated (%): C, 47.17; H, 5.60; N, 22.88; Na, 3.76; S, 2.41; C as carbonate, 0.0784. Found: C, 46.87; H, 5.57; N, 22.54; Na, 3.67; S, 2.27; C as carbonate, 0.078. SO_4^{2-}/CO_3^{2-} (mol/mol) = 11.5.

[Na$_2$(SO$_4$)$_{0.969}$(SeO$_4$)$_{0.031}$(L1)$_2$ (H$_2$O)$_4$]. FTIR (KBr): $\nu = 1095\,cm^{-1}$ (SO_4^{2-}), $870\,cm^{-1}$ (SeO_4^{2-}); analysis calculated (%): C, 46.92; H, 5.58; N, 22.80; Na, 3.74; S, 2.53; Se, 0.20. Found: C, 46.48; H, 5.49; N, 22.35; Na, 3.59; S, 2.36; Se, 0.195. SO_4^{2-}/SeO_4^{2-} (mol/mol) = 31.3.

[Na$_2$(SO$_4$)$_{0.67}$(CrO$_4$)$_{0.33}$(L1)$_2$ (H$_2$O)$_4$]. FTIR (KBr): $\nu = 1095\,cm^{-1}$ (SO_4^{2-}), 876, $893\,cm^{-1}$ (CrO_4^{2-}); analysis calculated (%): C, 46.73; H, 5.56; N, 22.70; Na, 3.73; S, 1.74; Cr, 1.39. Found: C, 46.43; H, 5.56; N, 22.36; Na, 3.64; S, 1.59; Cr, 1.33. SO_4^{2-}/CrO_4^{2-} (mol/mol) = 2.0.

[K$_2$(SO$_4$)$_{0.93}$(SeO$_4$)$_{0.07}$(L1)$_2$ (H$_2$O)$_2$]. FTIR (KBr): $\nu = 1098\,cm^{-1}$ (SO_4^{2-}), $868\,cm^{-1}$ (SeO_4^{2-}); analysis calculated (%): C, 47.00; H, 5.26; N, 22.84; S, 2.43; Se, 0.45. Found: C, 46.69; H, 4.90; N, 22.92; S, 2.15; Se, 0.41. SO_4^{2-}/SeO_4^{2-} (mol/mol) = 13.3.

[K$_2$(SO$_4$)$_{0.52}$(CrO$_4$)$_{0.48}$(L1)$_2$ (H$_2$O)$_2$]. FTIR (KBr): $\nu = 1098\,cm^{-1}$ (SO_4^{2-}), $878\,cm^{-1}$ (CrO_4^{2-}); analysis calculated (%): C, 46.76; H, 5.23; N, 22.72; K, 6.34; S, 1.35; Cr, 2.02. Found: C, 46.78; H, 5.16; N, 22.34; K, 5.92; S, 1.24; Cr, 1.90. SO_4^{2-}/CrO_4^{2-} (mol/mol) = 1.1.

Acknowledgement

This research was sponsored by the Division of Chemical Sciences, Geosciences and Biosciences, Office of Basic Energy Sciences, US Department of Energy.

References

(1) Gale, P.A. *Chem. Commun.* **2011**, *47*, 82–86.
(2) Gale, P.A. *Chem. Soc. Rev.* **2010**, *39*, 3746–3771.
(3) Sessler, J.L.; Gale, P.A.; Cho, W.-S. *Anion Receptor Chemistry*; Royal Society of Chemistry: Cambridge, UK, 2006.
(4) Park, C.H.; Simmons, H.E. *J. Am. Chem. Soc.* **1968**, *90*, 2431–2432.
(5) Graf, E.; Lehn, J.-M. *J. Am. Chem. Soc.* **1976**, *98*, 6403–6405.
(6) Kang, S.O.; Llinares, J.M.; Day, V.W.; Bowman-James, K. *Chem. Soc. Rev.* **2010**, *39*, 3980–4003.
(7) Ballester, P. *Chem. Soc. Rev.* **2010**, *39*, 3810–3830.
(8) Arunachalam, M.; Ghosh, P. *Chem. Commun.* **2011**, *47*, 8477–8492.
(9) Steed, J.W. *Chem. Soc. Rev.* **2009**, *38*, 506–519.
(10) Custelcean, R.; Bosano, J.; Bonnesen, P.V.; Kertesz, V.; Hay, B.P. *Angew. Chem. Int. Ed.* **2009**, *48*, 4025–4029.
(11) Custelcean, R. *Chem. Soc. Rev.* **2010**, *39*, 3675–3685.
(12) Custelcean, R.; Moyer, B.A. *Eur. J. Inorg. Chem.* **2007**, 1321–1340.
(13) Custelcean, R. *Curr. Opin. Solid State Mater. Sci.* **2009**, *13*, 68–75.
(14) Custelcean, R.; Gorbunova, M.G. *J. Am. Chem. Soc.* **2005**, *127*, 16362–16363.
(15) Custelcean, R.; Haverlock, T.J.; Moyer, B.A. *Inorg. Chem.* **2006**, *45*, 6446–6452.
(16) Wu, B.; Huang, X.; Xia, Y.; Yang, X.J.; Janiak, C. *CrystEngComm* **2007**, *9*, 676–685.
(17) Custelcean, R.; Sellin, V.; Moyer, B.A. *Chem. Commun.* **2007**, 1541–1543.
(18) Custelcean, R.; Jiang, D.E.; Hay, B.P.; Luo, W.; Gu, B. *Cryst. Growth Des.* **2008**, *8*, 1909–1915.
(19) Uzarevic, K.; Dilovic, I.; Matkovic-Calogovic, D.; Sisak, D.; Cindric, M. *Angew. Chem. Int. Ed.* **2008**, *47*, 7022–7025.
(20) Adarsh, N.N.; Kumar, D.K.; Dastidar, P. *CrystEngComm* **2008**, *10*, 1565–1573.
(21) Xia, Y.; Wu, B.; Liu, Y.; Yang, Z.; Huang, X.; He, L.; Yang, X.J. *CrystEngComm* **2009**, *11*, 1849–1856.
(22) Adarsh, N.N.; Kumar, D.K.; Dastidar, P. *CrystEngComm* **2009**, *11*, 796–802.
(23) Banerjee, S.; Adarsh, N.N.; Dastidar, P. *Eur. J. Inorg. Chem.* **2010**, 3770–3779.
(24) Wu, B.A.; Liang, J.J.; Zhao, Y.X.; Li, M.R.; Li, S.G.; Liu, Y.Y.; Zhang, Y.P.; Yang, X.J. *CrystEngComm* **2010**, *12*, 2129–2134.
(25) Adarsh, N.N.; Tocher, D.A.; Ribas, J.; Dastidar, P. *New J. Chem.* **2010**, *34*, 2458–2469.
(26) Custelcean, R.; Remy, P.; Bonnesen, P.V.; Jiang, D.E.; Moyer, B.A. *Angew. Chem. Int. Ed.* **2008**, *47*, 1866–1870.
(27) Custelcean, R.; Bock, A.; Moyer, B.A. *J. Am. Chem. Soc.* **2010**, *132*, 7177–7185.
(28) Wu, B.; Liang, J.; Yang, J.; Jia, C.; Yang, X.J.; Zhang, H.; Tang, N.; Janiak, C. *Chem. Commun.* **2008**, 1762–1764.
(29) Zhuge, F.Y.; Wu, B.A.; Liang, J.J.; Yang, J.; Liu, Y.Y.; Jia, C.D.; Janiak, C.; Tang, N.; Yang, X.J. *Inorg. Chem.* **2009**, *48*, 10249–10256.
(30) Rajbanshi, A.; Moyer, B.A.; Custelcean, R. *Cryst. Growth. Des.* **2011**, *11*, 2702–2706.
(31) Custelcean, R.; Remy, P. *Cryst. Growth. Des.* **2009**, *9*, 1985–1989.
(32) Custelcean, R.; Moyer, B.A.; Hay, B.P. *Chem. Commun.* **2005**, 5971–5973.